January 24, 2008

Controlled nanoparticle assembly through protein conformational changes

H Bayraktar
S Srivastava
CC You
VM Rotello
MJ Knapp

Soft Matter

www.softmatter.org

Volume 4 | Number 4 | 7 April 2008 | Pages 629–904

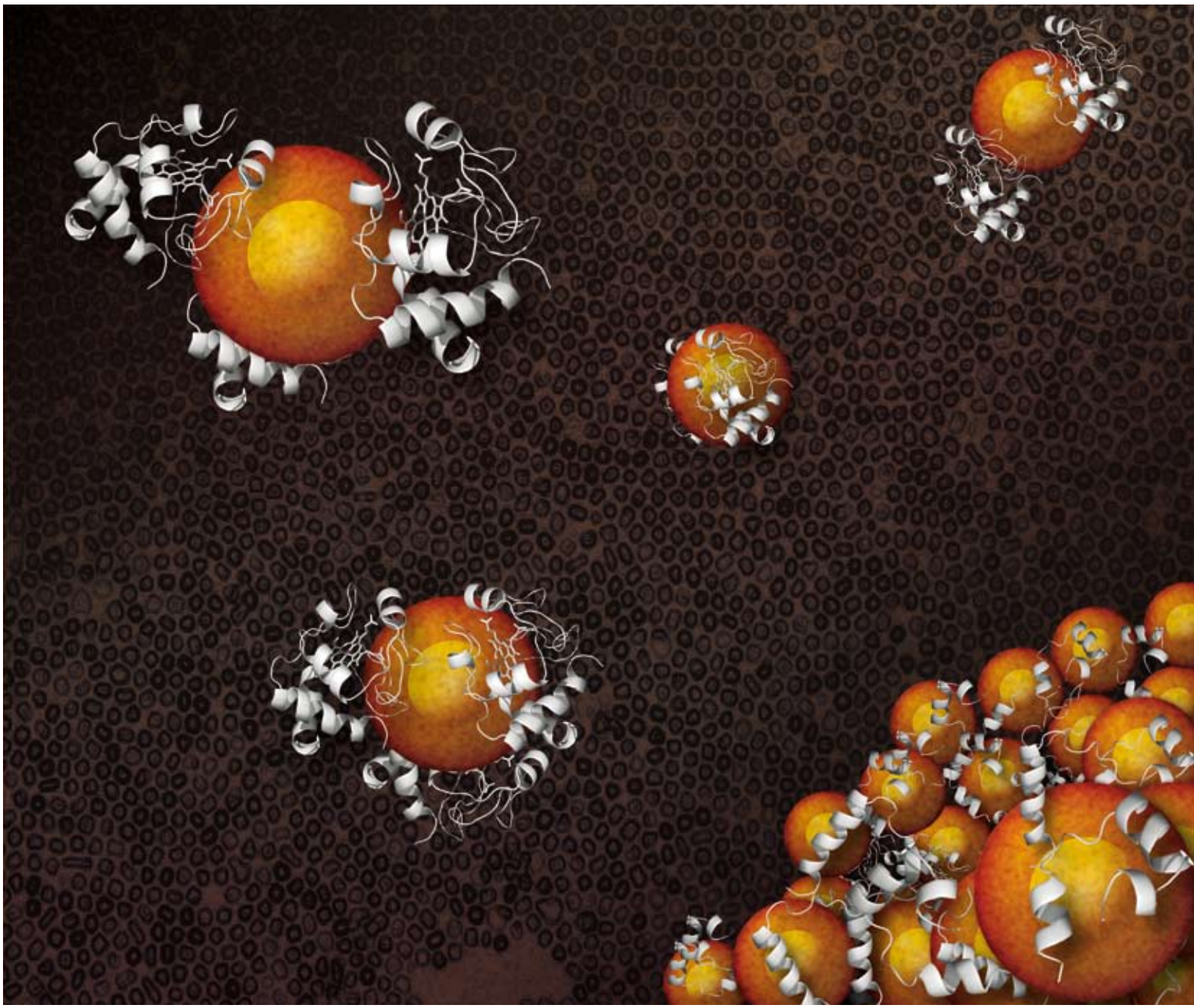

ISSN 1744-683X

RSC Publishing

1744-683X(2008)4:4;1-K

Controlled nanoparticle assembly through protein conformational changes

Halil Bayraktar,[a] Sudhanshu Srivastava,[a] Chang-Cheng You,[a] Vincent M. Rotello*[ab] and Michael J. Knapp*[ab]

Received 24th October 2007, Accepted 21st December 2007
First published as an Advance Article on the web 24th January 2008
DOI: 10.1039/b716386j

Selective surface recognition by proteins provides programmed bottom-up assembly of synthetic nanomaterials. We have investigated the controlled self-assembly of functionalized gold nanoparticles (**Au-TAsp**) with cytochrome *c* (Cyt *c*) and apoCyt *c* through complementary electrostatic interactions. **Au-TAsp** formed discrete, water-soluble adducts with native Cyt *c*, whereas unfolded apoCyt *c* induced nanocomposite formation at high Cyt *c* : **Au-TAsp** ratios. The binding of random-coil apoCyt *c* to **Au-TAsp** at low ratios induced α-helix formation in soluble nanocomposites, but at elevated ratios insoluble micron-scale aggregates were formed. The local structure of the assemblies was critically dependent on the Cyt *c* : **Au-TAsp** ratio. The dispersibility of apoCyt *c*–**Au-TAsp** was pH dependent, providing rapid and reversible control over nanocomposite assembly. The apoCyt *c*–**Au-TAsp** aggregates could likewise be disassembled through proteolytic cleavage of apoCyt *c*, demonstrating the ability to selectively remodel these hybrid materials.

Introduction

Recognition of biomolecular surfaces using nanoparticles provides a promising alternative route for assembling hybrid bionanomaterials.[1–8] As the physical properties of nanoparticles are distinct from those of bulk materials,[9–12] rational control over bottom-up assembly provides nanocomposites with unique physiochemical properties, offering new opportunities in electronics[13–15] and biosensing.[16,17] Engineering protein-based hybrid materials through biomolecular assembly, however, is challenging due to the complexities of protein-surface recognition. Two related approaches have generally been used for the creation of protein-based nanomaterials. The first approach utilizes genetically engineered peptides,[18] proteins,[19] and protein cages[20–24] to produce structures based on the recognition of inorganic surfaces by polypeptides.[25] In the second approach nanomaterial building blocks are arranged through the high-affinity recognition of covalently attached biomolecules, such as complementary oligonucleotides,[26,27] biotin and streptavidin,[28] or antibodies with antigens.[29–31] While the recognition in this case is specific, the high affinity binding of these systems often results in kinetically-controlled assembly, leading to disordered structures.

Cytochrome *c* (Cyt *c*) is a positively charged protein, with pI = 10,[32] that forms many transient protein–protein adducts of moderate binding affinity.[33–38] In contrast to the robust tertiary structure of Cyt *c*,[39,40] apoCyt *c* (formed by removing the heme of Cyt *c*) is predominately random coil while retaining the high positive charge of Cyt *c*. Nanoparticles carrying anionic surface functionalities can bind reversibly to Cyt *c*, altering protein stability[41–43] as well as forming hybrid materials with regular interparticle spacings.[44,45] We report herein the reversible assembly of negatively charged gold nanoparticles with apoCyt *c* into micron-scale aggregates. The Au nanoparticles (**Au-TAsp**) used in this study feature thiol ligands (**TAsp**) containing an aliphatic segment for nanoparticle stability, a tetra(ethylene glycol) segment to minimize nonspecific interactions, and a dianionic aspartate to provide a charged surface (Fig. 1c). With these particles, the conformation of Cyt *c* drastically alters the aggregation state of the nanoparticles. Discrete adducts are generated with natively folded Cyt *c* (Fig. 1). In contrast, apoCyt *c* exhibits considerable conformational flexibility, adopting native-like secondary structure, as well as providing tunable **Au-TAsp** spacing in nanocomposite aggregates of controlled size.

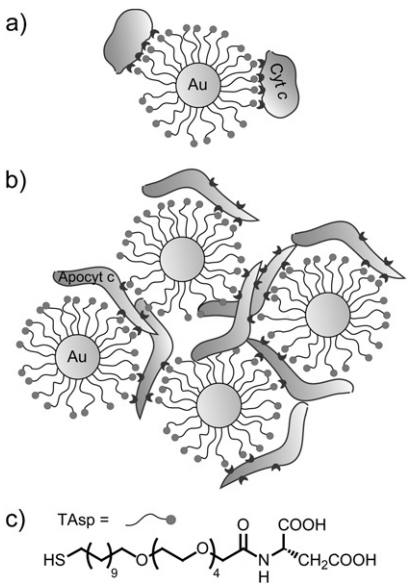

Fig. 1 Schematic representation of a) discrete adducts between **Au-TAsp** and native Cyt *c*; b) extended aggregates between **Au-TAsp** and apoCyt *c*; c) chemical structure of TAsp ligand.

[a]*Department of Chemistry, University of Massachusetts, 710 North Pleasant Street, Amherst, Massachusetts 01003, USA. E-mail: rotello@chem.umass.edu; mknapp@chem.umass.edu*
[b]*Program in Molecular and Cellular Biology, University of Massachusetts, 710 North Pleasant Street, Amherst, Massachusetts 01003, USA*

Results and discussion

Solution aggregation

Dynamic light scattering (DLS) was used to monitor assembly of **Au-TAsp** and Cyt *c*. The hydrodynamic diameter (D_H) of **Au-TAsp** was 8.2 ± 1.2 nm, consistent with 2 nm core diameter and fully extended **TAsp** ligands (3.2 nm[46]), while the D_H of Cyt *c* was 2.7 nm, in good accord with the crystallographically determined dimensions.[35,47] As Cyt *c* was mixed with **Au-TAsp** at increasing ratios (1 : 1 to 20 : 1), D_H increased monotonically from 10.2 to 15.1 nm (Fig. 2a and Table 1), indicating that the Cyt *c*–**Au-TAsp** adducts were discrete complexes in which a single **Au-TAsp** particle was surrounded by Cyt *c*.

In contrast to Cyt *c*, apoCyt *c* formed nanocomposites when mixed with **Au-TAsp** (Fig. 2b). At a 1 : 1 ratio, the D_H of the apoCyt *c*–**Au-TAsp** adduct was 10.6 ± 1.4 nm, similar to that observed for Cyt *c*. The adduct size increased at higher ratios, with an aggregate of roughly 1 μm forming at a 10 : 1 ratio. Interestingly, upon adding apoCyt *c* to a final ratio of 20 : 1, the D_H decreased to 0.1 μm, resulting in soluble aggregates.

Table 1 Adduct size at varied Cyt *c*:**Au-TAsp** ratio.

Cyt *c* : **Au-TAsp** ratio	D_H/nm of native Cyt *c*	D_H/nm of apoCyt *c*
0 : 1	8.2 ± 1.2	8.2 ± 1.2
1 : 1	10.2 ± 1.2	10.6 ± 1.4
4 : 1	12.2 ± 1.6	71 ± 12
10 : 1	13.7 ± 2.0	1010 ± 207
20 : 1	15.1 ± 2.1	98 ± 13

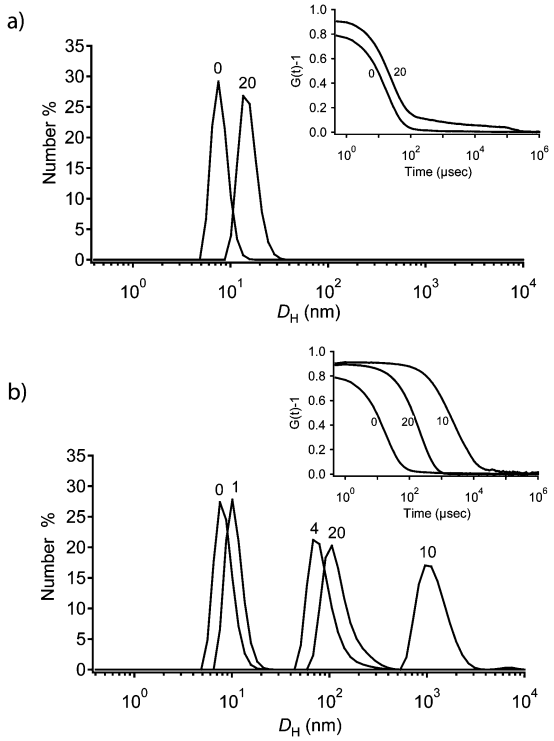

Fig. 2 DLS of a) Cyt *c*–**Au-TAsp** adducts; b) apoCyt *c*–**Au-TAsp** adducts at 0–20 fold excess of Cyt *c*. Insets show corresponding correlation functions.

The zeta potentials of the nanocomposites indicate that charge balance is key for aggregation. The zeta potential of **Au-TAsp** was −28.2 mV, due to the anionic surface ligands. Addition of Cyt *c* or apoCyt *c* (0–40 μM) to **Au-TAsp** (2 μM, 10mM Tris, pH 7.4) led to a positive shift in the zeta-potential, with an inflection point near a 10 : 1 ratio (Fig. 3a). As the charge of Cyt *c* at neutral pH is roughly +7,[32] and **Au-TAsp** has ∼100 anionic ligands,[48] this stoichiometry predominantly reflects charge balance. Cyt *c*–**Au-TAsp** complexes never reached neutrality, suggesting that the **Au-TAsp** surface was sterically crowded with Cyt *c* at higher Cyt *c*–**Au-TAsp** ratios. In contrast, apoCyt *c*–**Au-TAsp** exhibited a wide variation in zeta potential, such that insoluble aggregates with no net surface charge are formed at a 10 : 1 apoCyt *c* : **Au-TAsp** ratio (Fig. 3b). With excess apoCyt *c* the surface charge becomes positive, leading to smaller, soluble aggregates. The structural flexibility of apoCyt *c* was required for the formation of many of these aggregates, to overcome the steric limitations imposed by globular Cyt *c*.

The critical ratios of apoCyt *c* : **Au-TAsp** in the micron-scale aggregates were measured by DLS while varying solution pH

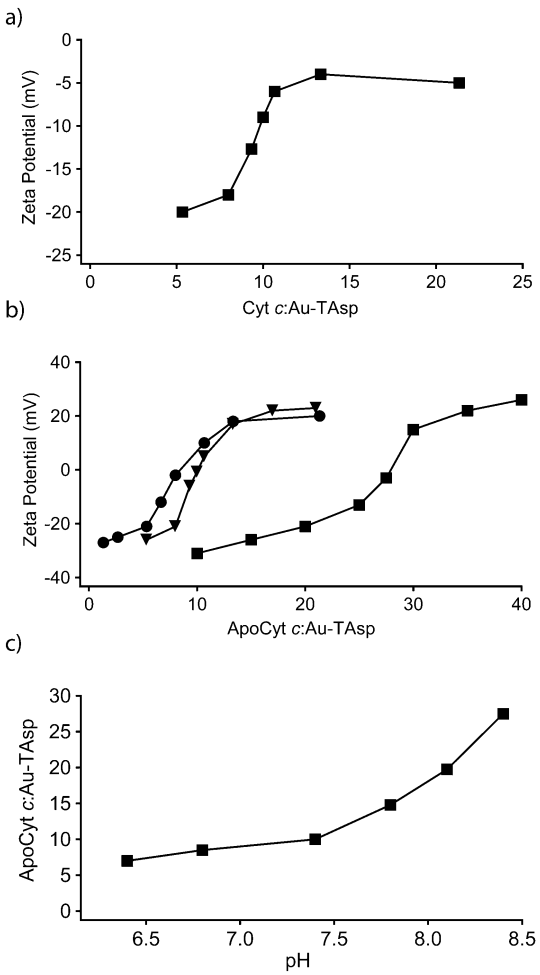

Fig. 3 Zeta potential of protein–**Au-TAsp** adducts at increasing protein ratios. a) Native Cyt *c*–**Au-TAsp** at pH 7.4; b) ApoCyt *c*–**Au-TAsp** complex at pH 6.4 (circles), 7.4 (triangles) and 8.4 (squares). c) Critical ratio of the apoCyt *c*–**Au-TAsp** micron-scale aggregate *vs.* pH. Lines drawn to guide the eye.

(Fig. 3c). This stoichiometry increased at higher pH values, consistent with deprotonation of lysine residues at pH > 8 leading to a smaller positive charge on apoCyt *c*. The critical ratios reflect the apoCyt *c* : **Au-TAsp** ratio in which charges are completely balanced, as aggregates formed below this critical ratio have an excess of the anioinic **Au-TAsp** leading to a negative zeta-potential, while those formed above this critical ratio have an excess of cationic apoCyt *c* leading to a positive zeta potential.

Conformational changes in Cyt *c*

The secondary structures of Cyt *c* and apoCyt *c* in the presence of **Au-TAsp** were investigated by circular dichroism (CD). The 2° structure of native Cyt *c* is predominantly α-helical, leading to distinct minima at 208 and 222 nm in CD spectra. The CD spectrum of native Cyt *c* changed slightly in the presence of **Au-TAsp** (Fig. 4a), indicating that the α-helical 2° structure was retained in the Cyt *c*–**Au-TAsp** adducts. ApoCyt *c*, however, exhibited significant conformational changes upon binding to **Au-TAsp**. ApoCyt *c* adopts a random coil conformation in solution, with a pronounced CD minimum at 202 nm. Upon binding to **Au-TAsp**, the CD spectrum of apoCyt *c* changed significantly, such that new minima appeared at 208 nm and 218 nm. This shifted CD spectrum indicates a more α-helical 2° structure for apoCyt *c* upon binding to **Au-TAsp** (Fig. 4b), and resembles a folding intermediate formed upon binding apoCyt *c* to phospholipid micelles.[49]

Transmission electron microscopy (TEM)

The morphology of the apoCyt *c*–**Au-TAsp** nanocomposites was investigated by transmission electron microscopy (TEM). **Au-TAsp** in the absence of apoCyt *c* was well dispersed (Fig. 5a), in accord with the monomeric particle size observed by DLS. A micron-scale aggregate was observed at a 10 : 1 apoCyt *c* : **Au-TAsp** ratio (Fig. 5b), consistent with the observation in solution. The morphology of the micron-scale aggregate was highly irregular, indicating a random assembly of ~10^6 **Au-TAsp** particles.† As expected, the sample composed of apoCyt *c* and **Au-TAsp** at a 20 : 1 ratio showed polydisperse smaller aggregates of ~100 nm diameter (Fig. 5c).

The TEM results confirm that while apoCyt *c* aggregates **Au-TAsp**, the apoCyt *c* : **Au-TAsp** ratio controls the size scale from 0.1 μm–1 μm. The nanocomposites formed from **Au-TAsp** with apoCyt *c* resemble those formed between nanoparticles and charged polymers,[50] suggesting that a flexible arrangement of compensating charges is essential for nanocomposite formation. Such flexibility would be absent in natively folded Cyt *c*, which may explain why native Cyt *c* fails to assemble **Au-TAsp** while unfolded Cyt *c* induces aggregation.

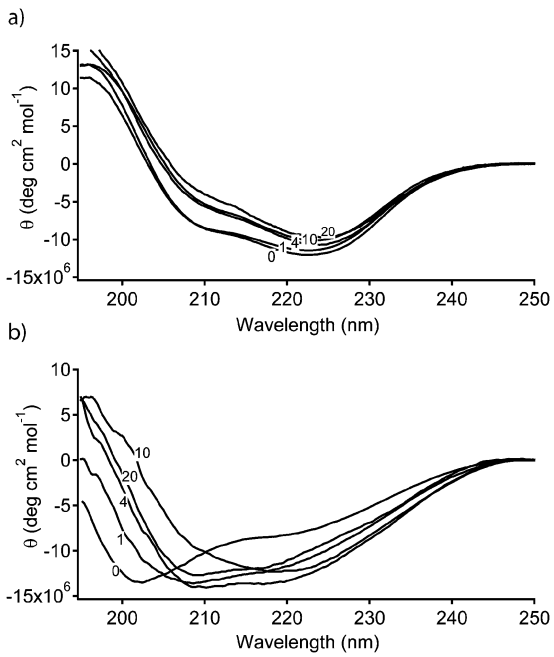

Fig. 4 Far-UV CD spectra at 23 °C of (a) Cyt *c* mixed with **Au-TAsp**; (b) apoCyt *c* mixed with **Au-TAsp**. Protein : **Au-TAsp** ratios as indicated.

Small angle X-ray scattering (SAXS)

SAXS was used to investigate the interparticle spacing of the nanocomposites, and provide a clearer picture of their internal structure. As a control, a solution of **Au-TAsp** was dried to a film and analyzed by SAXS, which indicated that the center-to-center nanoparticle spacing was $2\pi/q = 5.3$ nm. This spacing is somewhat smaller than expected for fully extended **TAsp** ligands, which may suggest ligand interdigitation between adjacent nanoparticles. The Cyt *c*–**Au-TAsp** adducts were shown by DLS to be discrete in solution; films were formed for SAXS analysis. At increasing loadings of native Cyt *c* (4, 10, 20 equivalents) the $2\pi/q$ smoothly increased from 5.9 nm to 7.7 nm (Fig. 6, 7), suggesting that the **Au-TAsp** cores are separated by a gear-like interdigitation of native Cyt *c*, as seen in a related study.[45] As the D_H for Cyt *c* is 2.7 nm, the overall increase in interparticle spacing suggests that higher Cyt *c* loadings lead to a more densely packed gear structure.

Solutions of the apoCyt *c*–**Au-TAsp** aggregates formed at elevated loadings of apoCyt *c* (4–20 equivalents) were dried to a film for SAXS analysis. The interparticle spacing smoothly increased from $2\pi/q = 6.0$ nm to 8.7 nm (Fig. 6, 7). These distances are slightly larger than observed for the native Cyt *c*–**Au-TAsp** adducts at identical ratios, suggesting that the protein tertiary structure dictates nanoparticle spacing. Despite the induced α-helical 2° structure, apoCyt *c* still packs less efficiently than native Cyt *c* in the nanocomposites.

pH- and protease-dependent disaggregation

As the apoCyt *c*–**Au-TAsp** nanocomposite is reversibly formed by the electrostatic attraction between the carboxylates of **TAsp** and the lysines of Cyt *c*, we reasoned that changes in pH would lead to changes in aggregation. The hydrodynamic diameter of the 10 : 1 apoCyt *c*–**Au-TAsp** nanocomposite was monitored by DLS while cycling between pH 7.4 and pH 10.8. The initial micron-scale aggregate ($D_H = 1100 \pm 250$ nm at pH 7.4) immediately decreased in size upon addition of base ($D_H = 8.7$

† A spherical nanocomposite of 1 μm diameter would have a volume of 5 × 10^8 nm^3. As the interparticle spacing within this nanocomposite is 9 nm, there will be one **Au-TAsp** per 360 nm^3 volume.

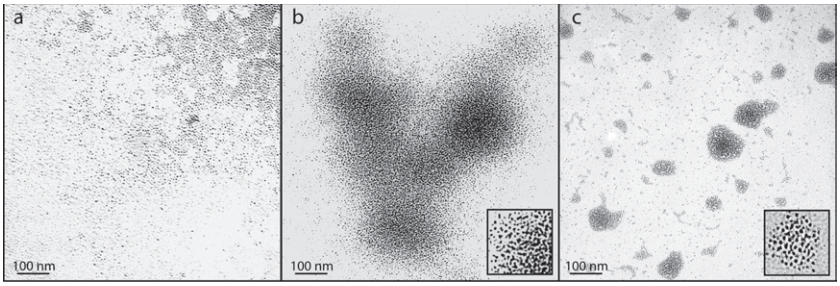

Fig. 5 Low-resolution TEM images (a) **Au-TAsp** in the absence of apoCyt *c*; (b) nanocomposites formed at a 10 : 1 apoCyt *c* : **Au-TAsp** ratio; (c) small aggregates from 20 : 1 apoCyt *c* : **Au-TAsp** ratio. Insets are 5 × magnification to show discrete **Au-TAsp** particles.

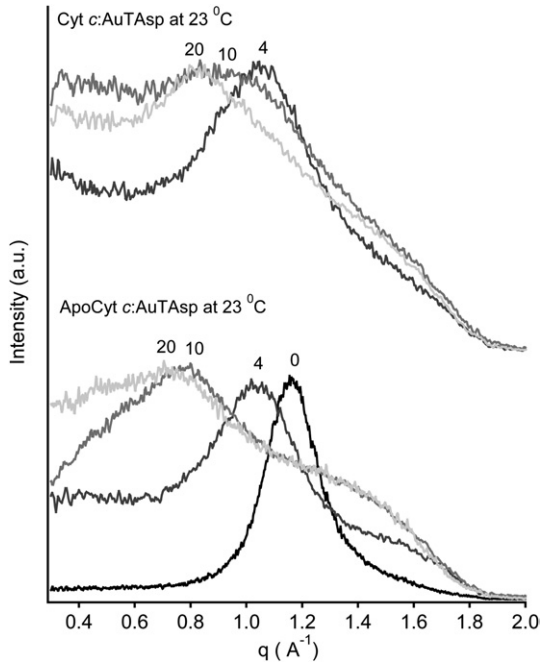

Fig. 6 Interparticle spacing within protein–nanoparticle adducts. a) Cyt *c* mixed with **Au-TAsp**; b) apoCyt *c* mixed with **Au-TAsp**.

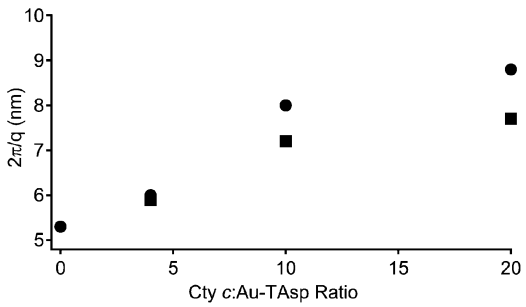

Fig. 7 Interparticle spacing ($2\pi/q$) as a function of the ratio of Cyt *c* : **Au-TAsp** (squares) and apoCyt *c* : **Au-TAsp** (circles).

± 2.4 nm at pH 10.8) (Fig. 8a). This disaggregation is attributed to deprotonation of lysine residues on apoCyt *c*. The addition of acid to pH = 7.4 led to re-aggregation (D_H = 1500 ± 280 nm). This process was repeated multiple times with little deviation in the hydrodynamic diameters, indicating that assembly was rapidly reversible under these conditions.

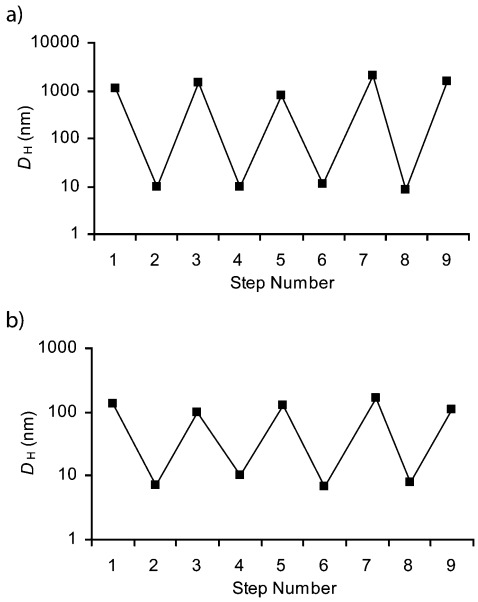

Fig. 8 Cycling of the hydrodynamic diameter of apoCyt *c*–**Au-TAsp** aggregates at pH 7.4 (odd steps) or pH 10.8 (even steps). apoCyt *c*–**Au-TAsp** at a ratio of (a) 10 : 1 and (b) 20 : 1.

The size of the smaller nanocomposites formed from a 20 : 1 apoCyt *c* : **Au-TAsp** ratio was also reversibly controlled by pH. The size of this nanocomposite (140 ± 36 nm at pH 7.4) immediately decreased upon addition of base (8.9 ± 2.2 nm at pH 10.8), indicating that the assembled nanoparticles became discrete (Fig. 8b). Added acid led to the reformation of the small nanocomposites, which was cycled through several pH changes.

Enzyme-mediated remodeling of the apoCyt *c*–**Au-TAsp** nanocomposite was shown by protease-induced disaggregation (Fig. 9). Trypsin, which cleaves the peptide bonds following lysine and arginine residues, was used to digest the nanocomposite formed at pH 7.4 from a 10 : 1 ratio of apoCyt *c* : **Au-TAsp**. D_H decreased over a period of six hours until the only products observed were discrete nanoparticles (D_H = 8.7 ± 1.6 nm). Clearly, the tryptic fragments of apoCyt *c* were too short to maintain the nanocomposite structure, suggesting a similarity to the nanoparticle assemblies formed with charged polymers.[50–52] Such enzyme-mediated disaggregation could be extended toward a controlled release strategy of appropriately formed nanocomposites containing therapeutic agents.

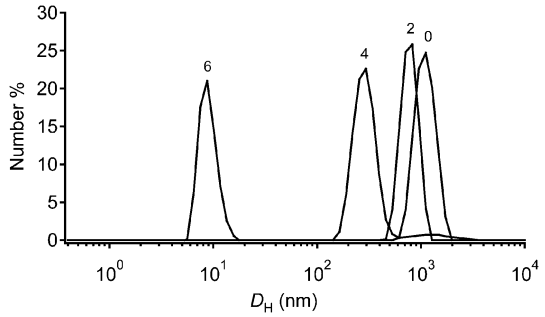

Fig. 9 Trypsin digestion of the micron-scale nanocomposite (10 : 1 apoCyt *c* : **Au-TAsp** ratio, pH 7.4) monitored by DLS. Time in hours indicated over each DLS scan.

Conclusions

Surface recognition is a promising route for the bottom-up assembly of nanomaterials. Through complementary electrostatic interactions with the functionalized gold nanoparticle **Au-TAsp**, apoCyt *c* and native Cyt *c* directed the assembly of composite nanomaterials of up to the micron length scale in a manner reminiscent of polymer-directed assembly of nanocomposites.[50] However, the use of a protein as the directing material in this case provided an added dimension for materials assembly, as the structure of Cyt *c* is better defined at the 2° and 3° levels than that of polymers. Conformational differences between apoCyt *c* and native Cyt *c* directly translated into distinct nanocomposites, as apoCyt *c*–**Au-TAsp** formed large aggregates, whereas native Cyt *c*–**Au-TAsp** consisted of discrete nanoparticles surrounded by multiple Cyt *c*. In addition, environmental stimuli such as pH change and protease digestion led to remodeling of the nanocomposites, suggesting their potential for controlled release applications.

Materials and methods

General

Horse heart Cyt *c* was obtained from Sigma-Aldrich Chemical Co. and used as received. ApoCyt *c* was prepared by removing the heme of Cyt *c* according to previously published methods,[53] stored at −80 °C, and thawed just before use. The extinction coefficient of apoCyt *c* at 277 nm was taken as 10 580 M^{-1} cm^{-1} for concentration determination.[54] **Au-TAsp** nanoparticles were synthesized using previously published methods.[48] All experiments, unless noted otherwise, were performed in Tris-HCl buffer (10 mM, pH = 7.4) at 23 °C.

Dynamic light scattering (DLS)

Samples were prepared using Tris-HCl buffer (10 mM, pH 7.4). The final concentration of **Au-TAsp** was 2 μM while the concentration of apoCyt *c* and Cyt *c* was varied from 2 to 40 μM. The nanoparticle–protein mixtures were diluted to 300 μL with buffer and incubated for 5 minutes prior to measurement with a MALVERN Zetasizer Nano ZS instrument using incident laser excitation at 633 nm. At least twelve measurements of the correlation time of scattered light intensity, $G(\tau)$, were averaged for each sample. The data were fitted to eqn (1), where B is baseline, A is amplitude, q is the scattering vector, τ is delay time and D is the diffusion coefficient:

$$G(\tau) = B + Ae^{-2q^2D\tau} \quad (1)$$

The hydrodynamic radius (R_H) of the scattering particles is inversely proportional to the diffusion coefficient D and the solvent viscosity (η), as shown in the Stokes–Einstein equation (eqn (2)), where k_B is Boltzmann's constant and T denotes the absolute temperature:

$$R_H = \frac{k_B T}{6\pi\eta D} \quad (2)$$

Zeta potential

Solutions containing **Au-TAsp** (2 μM) were mixed with apoCyt *c* (2.6 to 80 μM) in 10 mM Tris-HCl buffer at pH 6.4, 7.4 and 8.4. After incubation for five minutes, their zeta potentials were recorded on a MALVERN Zetasizer Nano ZS instrument.

pH dependence of micron-sized aggregate formation

Au-TAsp (2 μM final concentration) was mixed with varied concentrations of apoCyt *c* (2–75 μM final concentration) in Tris-HCl buffer (10 mM, pH 6.4). The final volume of all solutions was kept at 300 μL. Corresponding samples were prepared at pH 6.8, 7.4, 7.8, 8.0 and 8.4. The solutions were visually inspected, and those solutions near the turbidity point were selected for DLS measurements.

Circular dichroism (CD)

Stock solutions of apoCyt *c* (60 μM), Cyt *c* (60 μM), and **Au-TAsp** (7 μM) were prepared in Tris-HCl buffer (10 mM, pH 7.4). Cyt *c* (or apoCyt *c*) and **Au-TAsp** (final concentration of 1 μM) were then mixed at Cyt *c* : **Au-TAsp** ratios of 1 : 1 to 20 : 1. The CD spectra were recorded at 23 °C on a JASCO J-720 instrument, scanning from 195 to 250 nm at a rate of 50 nm min^{-1} with an average of three runs. The background of **Au-TAsp** was subtracted from the raw data, and the reported CD spectra were normalized to protein concentrations.

Small-angle X-ray scattering (SAXS)

Solutions containing **Au-TAsp** (3.2 μM) and apoCyt *c* or Cyt *c* (12.8–64.0 μM) were drop-cast onto 1 cm^2 kapton films placed at the bottom of a small vial and slowly dried. **Au-TAsp** particles in the absence of protein were dropcast on a Kapton film in a similar way.

Transmission electron microscopy (TEM)

TEM samples were prepared under similar conditions as the SAXS samples, with the exception that the films were drop-cast on carbon-coated copper grids (300 mesh). The samples were then analyzed on a JEOL 100CX electron microscope with an accelerating voltage of 100 keV.

pH-Dependent disaggregation

A 300 μL solution containing **Au-TAsp** (2 μM) and apoCyt *c* (20–40 μM) was prepared in Tris-HCl buffer (10 mM, pH 7.4).

The hydrodynamic diameters of the adducts were measured on a MALVERN Zetasizer Nano ZS instrument. The pH of the solution was increased to 10.8 by addition of 0.1 M NaOH, and the hydrodynamic diameter was measured after incubation for five minutes. Subsequently, the solution pH was lowered to 7.4 by addition of 0.1 M HCl, and the hydrodynamic diameter was measured after five minutes. This pH cycle was repeated four times.

Trypsin digestion

Bovine pancreas trypsin (type III) was purchased from Sigma-Aldrich Chemical Co. and used without further purification. A 400 μM stock solution was prepared by dissolving the lyophilized trypsin in Tris-HCl buffer (10 mM, pH 7.4). ApoCyt *c* and **Au-TAsp** were mixed at a 10 : 1 ApoCyt *c* : **Au-TAsp** ratio, and the hydrodynamic diameter was measured by DLS. Trypsin digestion was initiated by adding trypsin (25 μM) to the apoCyt *c*–**Au-TAsp** mixture, with the hydrodynamic diameter of the aggregate measured for six hours.

Acknowledgements

This research is supported by the University of Massachusetts – Amherst Research Council (MJK) and the National Institute and Health (VMR, GM 077173). The authors gratefully acknowledge the University of Massachusetts Materials Research Science and Engineering Center providing instruments and assistance for TEM and SAXS measurements.

References

1 M. Lundqvist, I. Sethson and B. H. Jonsson, *Langmuir*, 2004, **20**, 10639–10647.
2 B. P. Aryal and D. E. Benson, *Bioconjugate Chem.*, 2007, **18**, 585–589.
3 P. Roach, D. Farrar and C. C. Perry, *J. Am. Chem. Soc.*, 2006, **128**, 3939–3945.
4 S. S. Karajanagi, A. A. Vertegel, R. S. Kane and J. S. Dordick, *Langmuir*, 2004, **20**, 11594–11599.
5 E. Katz and I. Willner, *Angew. Chem., Int. Ed.*, 2004, **43**, 6042–6108.
6 C. C. You, A. Verma and V. M. Rotello, *Soft Matter*, 2006, **2**, 190–204.
7 P. Asuri, S. S. Bale, S. S. Karajanagi and R. S. Kane, *Curr. Opin. Biotechnol.*, 2006, **17**, 562–568.
8 R. S. Kane and A. D. Stroock, *Biotechnol. Prog.*, 2007, **23**, 316–319.
9 D. J. Norris, A. Sacra, C. B. Murray and M. G. Bawendi, *Phys. Rev. Lett.*, 1994, **72**, 2612–2615.
10 C. B. Murray, C. R. Kagan and M. G. Bawendi, *Annu. Rev. Mater. Sci.*, 2000, **30**, 545–610.
11 M. C. Daniel and D. Astruc, *Chem. Rev.*, 2004, **104**, 293–346.
12 A. P. Alivisatos, *Science*, 1996, **271**, 933–937.
13 W. P. Wuelfing, S. J. Green, J. J. Pietron, D. E. Cliffel and R. W. Murray, *J. Am. Chem. Soc.*, 2000, **122**, 11465–11472.
14 S. A. Maier, P. G. Kik, H. A. Atwater, S. Meltzer, E. Harel, B. E. Koel and A. A. G. Requicha, *Nat. Mater.*, 2003, **2**, 229–232.
15 D. J. Milliron, A. P. Alivisatos, C. Pitois, C. Edder and J. M. J. Frechet, *Adv. Mater.*, 2003, **15**, 58–61.
16 M. G. Sandros, D. Gao, C. Gokdemir and D. E. Benson, *Chem. Commun.*, 2005, 2832–2834.
17 J. M. Nam, S. I. Stoeva and C. A. Mirkin, *J. Am. Chem. Soc.*, 2004, **126**, 5932–5933.
18 S. R. Whaley, D. S. English, E. L. Hu, P. F. Barbara and A. M. Belcher, *Nature*, 2000, **405**, 665–668.
19 F. C. Meldrum, B. R. Heywood and S. Mann, *Science*, 1992, **257**, 522–523.
20 T. Douglas, E. Strable, D. Willits, A. Aitouchen, M. Libera and M. Young, *Adv. Mater.*, 2002, **14**, 415–418.
21 T. Douglas and M. Young, *Nature*, 1998, **393**, 152–155.
22 S. W. Lee, C. B. Mao, C. E. Flynn and A. M. Belcher, *Science*, 2002, **296**, 892–895.
23 M. T. Klem, D. Willits, D. J. Solis, A. M. Belcher, M. Young and T. Douglas, *Adv. Funct. Mater.*, 2005, **15**, 1489–1494.
24 J. Sun, C. DuFort, M. C. Daniel, A. Murali, C. Chen, K. Gopinath, B. Stein, M. De, V. M. Rotello, A. Holzenburg, C. C. Kao and B. Dragnea, *Proc. Natl. Acad. Sci. U. S. A.*, 2007, **104**, 1354–1359.
25 M. Sarikaya, C. Tamerler, A. K. Y. Jen, K. Schulten and F. Baneyx, *Nat. Mater.*, 2003, **2**, 577–585.
26 C. A. Mirkin, R. L. Letsinger, R. C. Mucic and J. J. Storhoff, *Nature*, 1996, **382**, 607–609.
27 A. P. Alivisatos, K. P. Johnsson, X. G. Peng, T. E. Wilson, C. J. Loweth, M. P. Bruchez and P. G. Schultz, *Nature*, 1996, **382**, 609–611.
28 S. Connolly and D. Fitzmaurice, *Adv. Mater.*, 1999, **11**, 1202–1205.
29 J. Yang, M. Mayer, J. K. Kriebel, P. Garstecki and G. M. Whitesides, *Angew. Chem., Int. Ed.*, 2004, **43**, 1555–1558.
30 W. Shenton, S. A. Davis and S. Mann, *Adv. Mater.*, 1999, **11**, 449–452.
31 C. M. Niemeyer, *Angew. Chem., Int. Ed.*, 2001, **40**, 4128–4158.
32 M. A. Marini, G. E. Marti, R. L. Berger and C. J. Martin, *Biopolymers*, 1980, **19**, 885–898.
33 H. B. Gray and J. R. Winkler, *Proc. Natl. Acad. Sci. U. S. A.*, 2005, **102**, 3534–3539.
34 M. R. Mauk, L. S. Reid and A. G. Mauk, *Biochemistry*, 1982, **21**, 1843–1846.
35 H. Pelletier and J. Kraut, *Science*, 1992, **258**, 1748–1755.
36 J. M. Nocek, J. S. Zhou, S. DeForest, S. Priyadarshy, D. N. Beratan, J. N. Onuchic and B. M. Hoffman, *Chem. Rev.*, 1996, **96**, 2459–2489.
37 F. Millett, in *Cytochrome c: A Multidisciplinary Approach*, ed. A. G. Mauk and R. A. Scott, University Science Books, Sausalito, CA, 1996, pp. 475–487.
38 H. R. Bosshard, in *Cytochrome c: A Multidisciplinary Approach*, ed. A. G. Mauk and R. A. Scott, University Science Books, Sausalito, CA, 1996, pp. 373–396.
39 A. Schejter, in *Cytochrome c: A Multidisciplinary Approach*, ed. A. G. Mauk and R. A. Scott, University Science Books, Sausalito, CA, 1996, pp. 335–345.
40 E. Margoliash and A. Schejter, in *Cytochrome c: A Multidisciplinary Approach*, ed. A. G. Mauk and R. A. Scott, University Science Books, Sausalito, CA, 1996, pp. 3–31.
41 H. Bayraktar, C. C. You, V. M. Rotello and M. J. Knapp, *J. Am. Chem. Soc.*, 2007, **129**, 2732–2733.
42 H. Bayraktar, P. S. Ghosh, V. M. Rotello and M. J. Knapp, *Chem. Commun.*, 2006, 1390–1392.
43 B. S. Sandanaraj, H. Bayraktar, K. Krishnamoorthy, M. J. Knapp and S. Thayumanavan, *Langmuir*, 2007, **23**, 3891–3897.
44 A. Verma, S. Srivastava and V. M. Rotello, *Chem. Mater.*, 2005, **17**, 6317–6322.
45 S. Srivastava, A. Verma, B. L. Frankamp and V. M. Rotello, *Adv. Mater.*, 2005, **17**, 617–621.
46 Chem3D, version 6.0, CyberChem, Gainesville, FL, 2000.
47 T. Takano and R. E. Dickerson, *J. Mol. Biol.*, 1981, **153**, 79–94.
48 C. C. You, M. De, G. Han and V. M. Rotello, *J. Am. Chem. Soc.*, 2005, **127**, 12873–12881.
49 S. E. Rankin, A. Watts and T. J. T. Pinheiro, *Biochemistry*, 1998, **37**, 12588–12595.
50 A. K. Boal, F. Ilhan, J. E. DeRouchey, T. Thurn-Albrecht, T. P. Russell and V. M. Rotello, *Nature*, 2000, **404**, 746–748.
51 A. K. Boal, T. H. Galow, F. Ilhan and V. M. Rotello, *Adv. Funct. Mater.*, 2001, **11**, 461–465.
52 B. L. Frankamp, O. Uzun, F. Ilhan, A. K. Boal and V. M. Rotello, *J. Am. Chem. Soc.*, 2002, **124**, 892–893.
53 W. R. Fisher, H. Taniuchi and C. B. Anfinsen, *J. Biol. Chem.*, 1973, **248**, 3188–3195.
54 E. Stellwagen, R. Rysavy and G. Babul, *J. Biol. Chem.*, 1972, **247**, 8074–8077.

